

Origin of magnetic frustration in $\text{Bi}_3\text{Mn}_4\text{O}_{12}(\text{NO}_3)$

Mojtaba Alaei,¹ Hamid Mosadeq,² Ismaeil Abdolhosseini Sarsari,¹ and Farhad Shahbazi^{1,*}

¹Department of Physics, Isfahan University of Technology, Isfahan 84156-83111, Iran.

²Department of Physics, Faculty of Science, Shahrekord University, Shahrekord 88186-34141, Iran.

(Dated: March 13, 2018)

$\text{Bi}_3\text{Mn}_4\text{O}_{12}(\text{NO}_3)$ (BMNO) is a honeycomb bilayers anti-ferromagnet, not showing any ordering down to very low temperatures despite having a relatively large Curie-Weiss temperature. Using ab initio density functional theory, we extract an effective spin Hamiltonian for this compound. The proposed spin Hamiltonian consists of anti-ferrimagnetic Heisenberg terms with coupling constants ranging up to third intra-layer and fourth inter-layer neighbors. Performing Monte Carlo simulation, we obtain the temperature dependence of magnetic susceptibility and so the Curie-Weiss temperature and find the coupling constants which best matches with the experimental value. We discover that depending on the strength of the interlayer exchange couplings, two collinear spin configurations compete with each other in this system. Both states have in plane Néel character, however, at small interlayer coupling spin directions in the two layers are antiparallel (N_1 state) and discontinuously transform to parallel (N_2 state) by enlarging the interlayer couplings at a first order transition point. Classical Monte Carlo simulation and density matrix renormalization group calculations confirm that exchange couplings obtained for BMNO are in such a way that put this material at the phase boundary of a first order phase transition, where the trading between these two collinear spin states prevents it from setting in a magnetically ordered state.

PACS numbers: 71.15.Mb, 75.50.Ee, 75.40.Mg.

$\text{Bi}_3\text{Mn}_4\text{O}_{12}(\text{NO}_3)$ (BMNO) is an experimental realization of frustrated honeycomb magnetic materials, synthesized by Smirnova et al. [1]. In this compound, the magnetic lattice can be effectively described by a weakly coupled honeycomb bilayers of Mn^{+4} ions (Fig. 1). The temperature dependence of magnetic susceptibility of BMNO does not indicate any ordering down to $T = 0.4\text{K}$, in spite of the Curie-Weiss temperature $\theta_{\text{CW}} \approx -257\text{K}$ [1, 2]. The absence of long-range ordering in BMNO is also confirmed by specific heat measurements [1, 2], neutron scattering [3] and high-field electron spin relaxation (ESR) experiments [4]. So far, the theoretical attempts to explain the magnetic properties of BMNO have been focusing on the frustration effect of second intra-layer coupling J_2 or the tendency toward dimerization by considering a large anti-ferromagnetic inter-layer nearest neighbor coupling J_{1c} [5–12]. In an attempt to calculate the exchange interactions by ab initio method, it is found that the dominant exchange interactions are nearest in-plane coupling (J_1) and also an effective inter-plane coupling (J_c) which exceeds J_1 [5]. However, in that work the experimental positions of the atoms in the structure are taken without geometry optimization and only 5 magnetic configurations are considered for the calculation of exchange interactions. In this paper, we obtain a Heisenberg spin Hamiltonian for BMNO, using an ab initio LDA+U calculation. In our calculations, we consider a detailed analysis of nonidentical Mn atoms which were assumed to be identical in the previous calculation [5]. We show that how this consideration can affect the exchange couplings in the spin Hamiltonian. We find that in contrary to the previous works, none of J_2 and J_{1c} are large enough to frustrate BMNO to reach an ordered

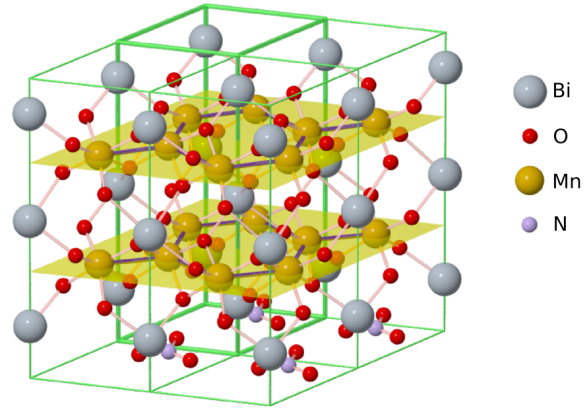


FIG. 1. (Color online) The 2×2 supercell of BMNO. The thicker green lines show the primitive cell. Two (yellow transparent) planes show honeycomb lattices which are made of Mn atoms.

state. Indeed, surprisingly the interlayer coupling constants are finely tuned in a way that make this system living at the edge boundary of two competing magnetic states.

Ab initio method. To derive magnetic exchange couplings, we employ Density Functional Theory (DFT) with Full-Potential Local-Orbital minimum-basis (FPLO), using FPLO code [13] (FPLO14.00-45). For charge analysis we employ Projector Augmented Wave (PAW) method, using Quantum-Espresso (QE) distribution [14]. To account for exchange-correlation interaction we use PBE functional [15] from Generalized Gradient Approximation (GGA). To improve estimation of electron-electron Coulomb interactions, we also

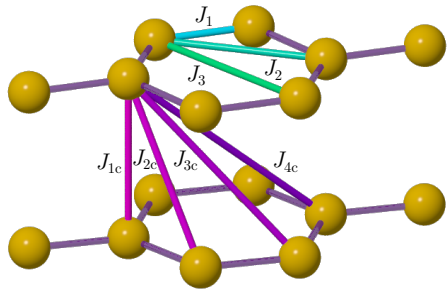


FIG. 2. J_1 , J_2 and J_3 indicate the Heisenberg exchange coupling constants between first, second and third nearest neighbor in-plane Mn^{+4} ions, respectively. J_{1c} , J_{2c} , J_{3c} and J_{4c} indicate the Heisenberg exchange coupling constants between inter-plane first, second and third nearest neighbor Mn^{+4} ions, respectively.

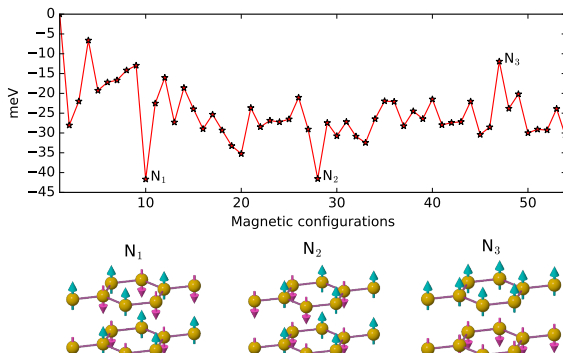


FIG. 3. (Color online) (top): The ab initio energy landscape (per Mn atom) of 54 magnetic configurations obtained by DFT+ U with $U = 1.5$ eV. The energies of magnetic configurations are respect to fully ferromagnetic state whose energy is set to 0. (bottom): Three magnetic configurations N_1 , N_2 and N_3 .

add Hubbard-like U correction to DFT calculations, i.e., DFT+ U [16, 17]. To implement DFT+ U , FPLO uses Liechtenstein's approach [18, 19]. In Liechtenstein's approach the two parameters, U (on-site Coulomb repulsion) and J_H (the on-site Hund exchange) needs to be set, which we use $J_H = 1.0$ eV and $U = 1.5, 2.0, 3.0$ and 4.0 eV.

Spin Hamiltonian. The strategy of finding an effective spin Hamiltonian from ab initio calculations is to first compute the ground state energy for some given magnetic configurations. Then, mapping the energy difference of these configurations to an appropriate spin model gives us the coupling constants of the model. In this work, we use non-relativistic DFT, hence any magnetic anisotropy originating from the spin-orbit interaction is ignored in this approximation. Therefore, to leading order, we pro-

pose a spin Hamiltonian containing only bi-linear Heisenberg interactions, $\mathcal{H}_{\text{Heisenberg}} = \sum_{i>j} J_{ij} \mathbf{n}_i \cdot \mathbf{n}_j$, where \mathbf{n}_i and \mathbf{n}_j are classical unit vectors representing the orientation of the magnetic moments at sites i and j , respectively, with exchange interactions J_{ij} between them. The primitive cell of $\text{Bi}_3\text{Mn}_4\text{O}_{12}(\text{NO}_3)$ contains 23 atoms. Because of the limitation in computational resources, we use the 2×2 supercell containing 92 atoms (Fig. 1). This lets us calculate J_{ij} 's up to the third in-plane neighbor (J_1 , J_2 and J_3) and up to the fourth inter-plane neighbor coupling (J_{1c} , J_{2c} , J_{3c} and J_{4c}) (see figure 2). BMNO is metallic in GGA, however, implementing spin-polarized calculation makes this compound insulating, independent of its magnetic configuration. Within co-linear spin polarized GGA, the ground state is a Néel state in which the nearest neighbor Mn magnetic moments (in and out of plane) are anti-parallel with respect to each other. This magnetic configuration is marked by N_1 in Fig. 3. We calculated the total energy for more than 50 independent magnetic configurations. Then employing the least square method, enables us to obtain the exchange couplings with the accuracy of 0.02 meV. The top panel of figure 3 represents the energy landscape (per Mn atom) calculated for 54 different magnetic configurations within the super-cell shown in Fig. 1. The detailed description of these configurations is given in Ref.[20]. As it is obvious from this figure, the two configurations N_1 and N_2 (bottom panel of Fig. 3) are very close in energy space. In configuration N_2 , the magnetic ordering in each honeycomb layer is Néel type, but unlike N_1 , the magnetic moment orientations of two layer are parallel. The coupling constants of the Heisenberg Hamiltonian, obtained by different values of on-site Coulomb interaction U , are given in Table I. We also checked that the exchange interactions between the adjacent honeycomb bilayers are negligible comparing to the ones inside the bilayers [20]. It is important to mention that to achieve equal couplings between equivalent Mn ions in the two layers, we need to geometrically optimize the atomic positions rather than just using the experimental atomic positions (for the details see supplementary information [20]).

The Mn spin state. The bond valence sum indicates the valence state $\text{Bi}_3^{3+}\text{Mn}_4^{4+}\text{O}_{12}^{2-}(\text{NO}_3)^-$ for BMNO [1]. However, using the charge analyzing code Critic2 [21, 22], within GGA/PAW, we find the valence state $\text{Bi}_3^{1.96+}\text{Mn}_4^{1.87+}\text{O}_{12}^{1.04-}(\text{NO}_3)^{0.86-}$ in N_1 -configuration. This charge distribution will not change dramatically in the case of implementing DFT+ U even with large U parameter. We also made sure that using an all-electron method, such as FPLO, this picture of charge distribution remains nearly unchanged. The local density analysis (Lowdin charges), also proposes the charge distribution $\text{Bi}_3^{1.49+}\text{Mn}_4^{1.45+}\text{O}_{12}^{0.74-}(\text{NO}_3)^{0.40-}$. These charge analyses show that the Mn-O bonds are ionic-covalent instead of being completely ionic. Indeed, the reason for such a fractional charge distribution in BMNO

TABLE I. Heisenberg constants obtained by ab initio calculations (LDA+ U) using different U . The geometrically optimized structure (in the ferromagnetic state) is used in these calculations. The last column shows Curie-Weiss temperature obtained from Monte Carlo simulations for a system size with $N = 4 \times 24 \times 24 \times 1$. The experimental Curie-Weiss temperature is between -257K [1] and -222K [2].

| method | $U(\text{eV})$ | $J_1(\text{meV})$ | $J_2(\text{meV})$ | $J_3(\text{meV})$ | $J_{1c}(\text{meV})$ | $J_{2c}(\text{meV})$ | $J_{3c}(\text{meV})$ | $J_{4c}(\text{meV})$ | $\Theta_{CW}(K)$ |
|--------|----------------|-------------------|-------------------|-------------------|----------------------|----------------------|----------------------|----------------------|------------------|
| FPLO | 1.5 | 10.7 | 0.9 | 1.2 | 3.0 | 1.1 | 0.5 | 0.9 | -244 |
| | 2.0 | 9.0 | 0.8 | 1.0 | 2.6 | 0.9 | 0.5 | 0.8 | -203 |
| | 3.0 | 6.6 | 0.6 | 0.8 | 2.1 | 0.7 | 0.3 | 0.6 | -144 |
| | 4.0 | 5.1 | 0.5 | 0.6 | 1.7 | 0.6 | 0.3 | 0.5 | -111 |

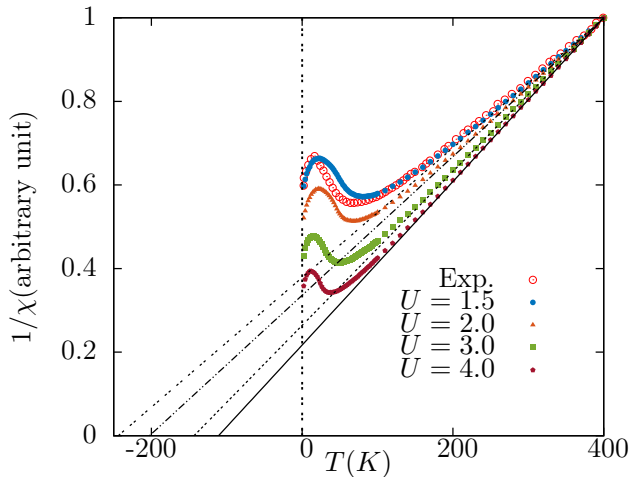


FIG. 4. (Color online) Temperature dependence of the inverse normalized DC susceptibility ($1/\chi$) of BMNO obtained in experiment and MC simulations for different set of ab initio exchange couplings derived by using $U = 1.5 \text{ eV}$ (filled circles), $U = 2.0 \text{ eV}$ (triangles), $U = 3.0 \text{ eV}$ (squares) and $U = 4.0 \text{ eV}$ (pentagons). The experimental data (empty circles) is extracted from figure 7 of Ref. [1]. For the normalization, all the data are divided by their values at $T = 400$. The crossing of the line fitted at high temperatures to $1/\chi$ with the horizontal axis gives the Curie-Weiss temperature.

is the strong hybridization between Mn d-orbitals and the neighboring O p-orbitals. This also lowers the magnetic moment of Mn ions from $3\mu_B$ to about $2.5\mu_B$ (see Table I in supplementary information [20]).

Monte Carlo Simulations. To gain insight into the finite temperature properties of the model Hamiltonian, we perform MC simulation. MC simulations are done on a $24 \times 24 \times 1$ supercell contains 2304 Mn atoms with periodic boundary conditions. We use single spin Metropolis updating, 3×10^6 MC steps for thermalization and 7×10^6 MC samplings for the measurement of physical quantity. To reduce the correlations, we skip 5 MC sweeps between successive data collections. In Figure 4 the temperature dependence of inverse magnetic susceptibility for the sets of exchange couplings obtained by ab initio method using $U = 1.5, 2.0, 3.0, 4.0 \text{ eV}$ and also the experimental values are compared. This figure shows a very good agreement

between the experimental values and the set of exchanges obtained by using $U = 1.5 \text{ eV}$. The linear fit at high temperatures crosses the T -axis at a negative value which is the Curie-Weiss temperature θ_{CW} . It can be seen that θ_{CW} increases by increasing the value of onsite Coulomb repulsion U . The $\theta_{CW} = -244\text{K}$ is closest to what has been measured experimentally. To speculate about the ground state of the Hamiltonian, we calculated the interlayer spin-spin correlation at a low temperature, up to fourth neighbor (Fig. 5). The correlations are calculated by averaging over 5×10^4 MC samplings at $T = 2\text{K}$. As it can be seen from this figure, for the couplings corresponding to $U = 1.5 \text{ eV}$ (Table I), the spin-spin correlations between the two layers are very small. We observe that, increasing (decreasing) the value of interlayer coupling by a little amount pushes the system toward N_1 (N_2) type ordering. Figure 5 shows the change of spin-spin correlation patterns, when J_{2c} varies by only ± 5 percent, while keeping the rest of the couplings unchanged. The

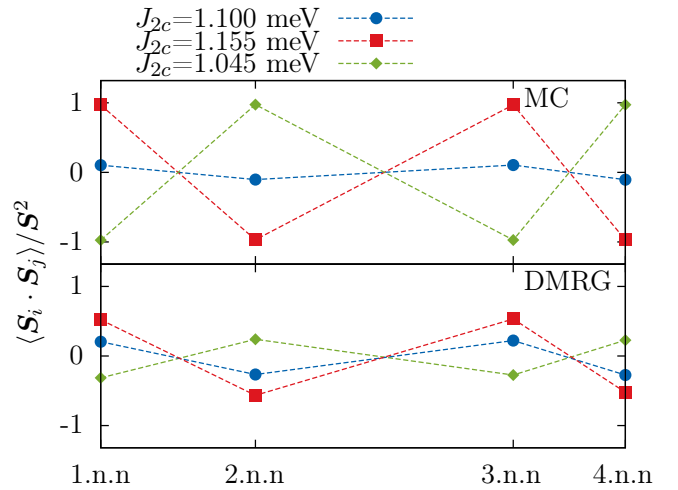


FIG. 5. (Color online) Interlayer spin-spin correlation up to neighbor obtained by (top) MC simulation, (bottom) DMRG (normalized by S^2). $J_1, J_2, J_3, J_{1c}, J_{3c}$ and J_{4c} are kept fixed at those found by $U = 1.5 \text{ eV}$. The spin-spin correlations at $J_{2c} = 1.100 \text{ meV}$ are obtained by using $U = 1.5 \text{ eV}$ (blue circles) and compared with $J_{2c} = 1.045$ (green diamonds) and $J_{2c} = 1.155 \text{ meV}$ (red squares).

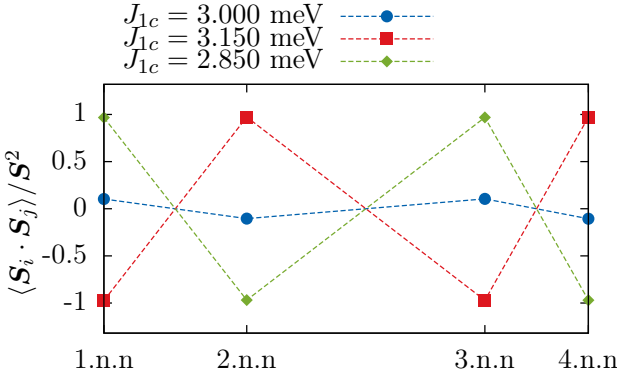


FIG. 6. (Color online) Interlayer spin-spin correlation (normalized by S^2) up to fourth neighbor obtain by MC simulation. $J_1, J_2, J_3, J_{2c}, J_{3c}$ and J_{4c} are kept fixed at the values obtained by $U = 1.5$ eV. The spin-spin correlations at $J_{2c} = 3.0$ meV are obtained by using $U = 1.5$ eV (blue circles) and compared with $J_{1c} = 3.15$ (red squares) and $J_{1c} = 2.85$ meV (green diamonds).

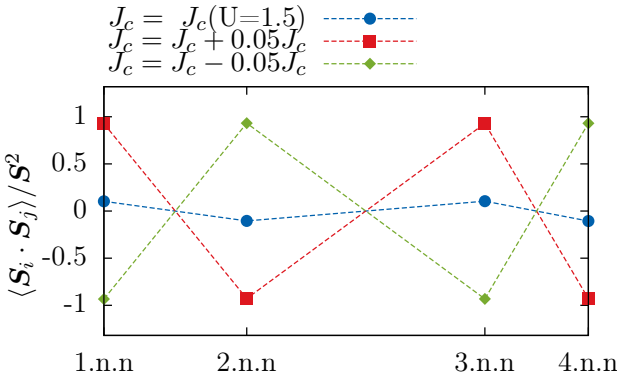


FIG. 7. (Color online) Interlayer spin-spin correlation (normalized by S^2) up to fourth neighbor obtain by MC simulation. J_1, J_2, J_3 are kept fixed at the values obtained using $U = 1.5$ eV. The spin-spin correlations for the interlayer coupling calculated at $U = 1.5$ (blue circles) are compared with the ones increased (red squares) and decreased (green diamonds) by 5 percent.

same results are obtained when only J_{1c} is changed while the other couplings are fixed (Fig. 6) and also in the case that all the interlayer couplings are shifted up or downward (Fig. 7). We also found that the small changes in the in-plane couplings do not induce spin ordering in the system.

Quantum effects. To make an inquiry about the quantum correlations at zero temperature, we use the density matrix renormalization group (DMRG) technique based on a matrix product state representation to evaluate the spin correlations functions [23]. In our calculations, we adopt $S = 3/2$ (which is the spin of Mn^{+4}) and the lattices with $4 \times L^2$ sites with $L = 4$. The spin-spin corre-

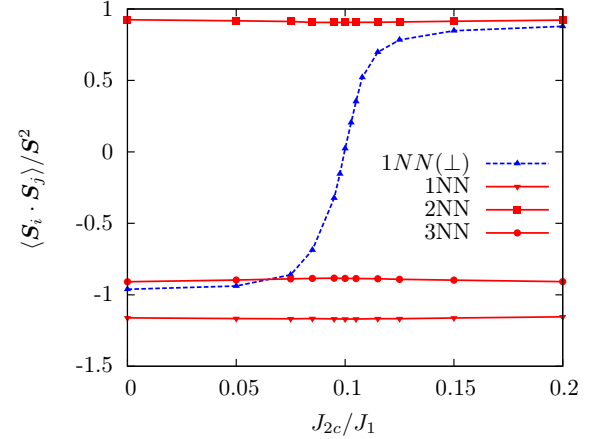


FIG. 8. (Color online) DMRG results for the variation of spin-spin correlations for first, second, third in-plane neighbors and first inter-plane neighbors versus J_{2c}/J_1 . Other coupling are fixed by those obtained by $U = 1.5$ eV.

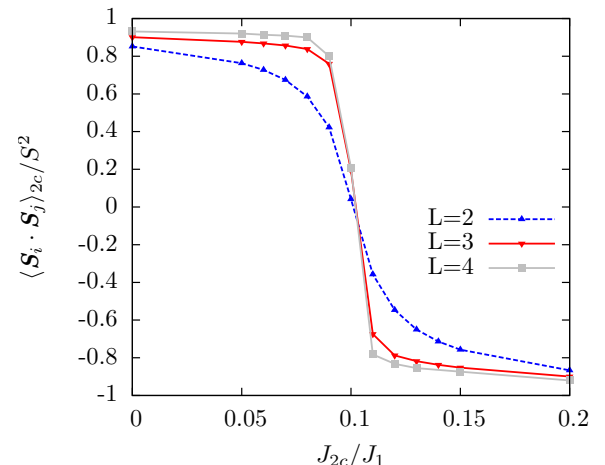


FIG. 9. (Color online) DMRG results for the variation of the second interlayer spin-spin correlations versus J_{2c}/J_1 , for lattices of size $4 \times L^2$ with $L = 2, 3, 4$. Other coupling are fixed by those obtained by $U = 1.5$ eV.

lations normalized by S^2 (shown in the bottom panel of Fig. 5), confirms the transition from N_1 to N_2 states at $J_{2c}/J_1 \sim 0.1$, despite the weakening of the correlations as the effect of quantum fluctuations. This is while, the in-plane spins are in the Néel state, independent of the value of J_{2c} (Fig. 8).

Now, we proceed to determine the order of $\text{N}_1\text{-}\text{N}_2$ transition for the set of exchange interactions obtained by using $U = 1.5$ eV. Using Feynman-Hellmann theorem, the first derivative of the ground state energy with respect to a control parameter, say J_{2c} , is given by

$$\frac{\partial E_0}{\partial J_{2c}} = \langle \frac{\partial H}{\partial J_{2c}} \rangle = \frac{3}{2} N \langle \mathbf{S}_i \cdot \mathbf{S}_j \rangle_{2c}, \quad (1)$$

in which $N = 4L^2$ is the number of lattice points in a bilayer honeycomb of linear size L and $\langle \mathbf{S}_i \cdot \mathbf{S}_j \rangle_{2c}$ denotes the spin-spin correlation between the second interlayer neighbors. Figure 9 represents the DMRG results for the variation of this correlation versus J_{2c}/J_1 , for the lattices of linear sizes $L = 2, 3, 4$. This figure shows a discontinuity in the second interlayer neighbor spin-spin correlation which becomes more pronounced by increasing the size of the system. Therefore equation 1 implies that the phase transition between these two ordered states is first order. Indeed, this result was expected because of different symmetries of N_1 and N_2 states.

Conclusion. In summary, we employed an ab initio LDA+U method to obtain the exchange coupling constants of a spin Hamiltonian for describing the magnetic properties of the honeycomb bilayer BMNO and figure out the reason that this compound does not show any ordering down to very low temperatures. Using $U = 1.5$ eV, we found that a Hamiltonian containing only bilinear Heisenberg terms up to third in-plane and fourth out of plane neighbor, well matches the measured DC magnetic susceptibility for this material. Classical MC simulations and DMRG calculations on this spin Hamiltonian shows no sign of long-range ordering down to zero temperature. It is surprising that in BMNO the interlayer couplings are tuned in such a way to let this compound living at the phase boundary of the two collinear magnetic configurations N_1 and N_2 . Indeed, the interlayer coupling J_{1c} and J_{3c} encourage the N_1 ordering, while J_{2c} and J_{4c} favor the N_2 state. Therefore, the balance between these two sets of couplings adjusts BMNO to be at the N_1 - N_2 phase boundary. Hence, in the presence of any imbalance created as the effect of tension, compressive pressure, chemical doping, etc, the transition to N_1 or N_2 ordered states is expected. At this very special point, the spin-spin correlations in each layer are Néel type, however, there is almost a vanishing correlation between the two layers, making the dynamics of the two Néel states uncorrelated. The lack of correlations between the adjacent layer makes BMNO an effectively two-dimensional Heisenberg system for which there would be no finite temperature phase transition, according to the Mermin-Wagner theorem. It is also worthy to note that the presence of a strong enough spin-lattice interaction, could induce a spin-peierls lattice distortion and hence resolve the spin frustration. However, the reason that such a transition has not been observed experimentally, could be due to the small spin-orbit interaction in Mn atom which makes the temperature scale corresponding to the magneto-elastic interaction too small to cause an observable static lattice distortion in BMNO down to 50 mK.

We acknowledge Michel Gingras, Jeff Rau and Stefano de Gironcoli for the most useful discussions and comments. We also thank Phivos Mavropoulos for providing us with his MC code. DMRG results were checked by

using the ALPS **mps-optim** application.

* shahbazi@cc.iut.ac.ir

- [1] O. Smirnova, M. Azuma, N. Kumada, Y. Kusano, M. Matsuda, Y. Shimakawa, T. Takei, Y. Yonesaki, and N. Kinomura, *Journal of the American Chemical Society* **131**, 8313 (2009).
- [2] N. Onishi, K. Oka, M. Azuma, Y. Shimakawa, Y. Motome, T. Taniguchi, M. Hiraishi, M. Miyazaki, T. Matsuda, A. Koda, *et al.*, *Physical Review B* **85**, 184412 (2012).
- [3] M. Matsuda, M. Azuma, M. Tokunaga, Y. Shimakawa, and N. Kumada, *Phys. Rev. Lett.* **105**, 187201 (2010).
- [4] S. Okubo, F. Elmasry, W. Zhang, M. Fujisawa, T. Sakurai, H. Ohta, M. Azuma, O. A. Smirnova, and N. Kumada, *Journal of Physics: Conference Series* **200**, 022042 (2010).
- [5] H. C. Kandpal and J. van den Brink, *Physical Review B* **83**, 140412 (2011).
- [6] R. Ganesh, D. Sheng, Y.-J. Kim, and A. Paramakanti, *Physical Review B* **83**, 144414 (2011).
- [7] R. Ganesh, S. V. Isakov, and A. Paramakanti, *Physical Review B* **84**, 214412 (2011).
- [8] J. Oitmaa and R. Singh, *Physical Review B* **85**, 014428 (2012).
- [9] S. Okubo, T. Ueda, H. Ohta, W. Zhang, T. Sakurai, N. Onishi, M. Azuma, Y. Shimakawa, H. Nakano, and T. Sakai, *Phys. Rev. B* **86**, 140401 (2012).
- [10] H. Zhang, M. Arlego, and C. Lamas, *Physical Review B* **89**, 024403 (2014).
- [11] F. G. Albarracín and H. Rosales, *Physical Review B* **93**, 144413 (2016).
- [12] R. Bishop and P. Li, arXiv preprint arXiv:1611.03287 (2016).
- [13] K. Koepernik and H. Eschrig, *Phys. Rev. B* **59**, 1743 (1999).
- [14] P. Giannozzi *et al.*, *Journal of Physics: Condensed Matter* **21**, 395502 (2009).
- [15] J. P. Perdew, K. Burke, and M. Ernzerhof, *Phys. Rev. Lett.* **77**, 3865 (1996).
- [16] V. I. Anisimov, J. Zaanen, and O. K. Andersen, *Phys. Rev. B* **44**, 943 (1991).
- [17] V. I. Anisimov, I. V. Solovyev, M. A. Korotin, M. T. Czyżyk, and G. A. Sawatzky, *Phys. Rev. B* **48**, 16929 (1993).
- [18] A. I. Liechtenstein, V. I. Anisimov, and J. Zaanen, *Phys. Rev. B* **52**, R5467 (1995).
- [19] H. Eschrig, K. Koepernik, and I. Chaplygin, *Journal of Solid State Chemistry* **176**, 482 (2003), special issue on The Impact of Theoretical Methods on Solid-State Chemistry.
- [20] See Supplementary Material at [URL].
- [21] A. O. de-la Roza, E. R. Johnson, and V. Luua, *Computer Physics Communications* **185**, 1007 (2014).
- [22] A. O. de-la Roza, M. Blanco, A. M. Pends, and V. Luua, *Computer Physics Communications* **180**, 157 (2009).
- [23] M. Dolfi, B. Bauer, S. Keller, A. Kosenkov, T. Ewart, A. Kantian, T. Giamarchi, and M. Troyer, *Computer Physics Communications* **185**, 3430 (2014).

SUPPLEMENTAL MATERIAL

CHARGE ANALYSIS

In this section, we explain why Mn-O bonds has ionic-covalent character. In fact, the ionic-covalent character of Mn-O bonds can be observed in the hybridization of Mn-*d* and O-*p* orbitals. The point group of MnO₆ clusters in Bi₃Mn₄O₁₂(NO₃) is *C*₃, where the *C*₃-axis is perpendicular to honeycomb layer. Therefore, the Mn-*d* orbitals are splitted as the effect of the crystal field into d_{z^2} , (d_{xz}, d_{yz}) and ($d_{xy}, d_{x^2-y^2}$). The projected density of states plotted in figure 10 together with the orbital occupation calculation shown in Table. II, indicate that the hybridization among *d* orbitals of Mn and *p* orbitals of O makes the crystal field states (d_{xz}, d_{yz}) and ($d_{xy}, d_{x^2-y^2}$) to have fractional occupations. Therefore the bond va-

TABLE II. Charge distribution among Mn-*d* orbitals obtained by GGA/PAW Lowdin charge analysis.

| spin | d_{tot} | d_{z^2} | (d_{xz}, d_{yz}) | ($d_{xy}, d_{x^2-y^2}$) |
|------|-----------|-----------|----------------------|---------------------------|
| ↑ | 3.8456 | 0.9825 | 0.6296 | 0.8020 |
| ↓ | 1.2960 | 0.1890 | 0.2914 | 0.2621 |

lence sums (Bi³⁺Mn⁴⁺O²⁻₁₂(NO₃)⁻) [1] does not give rise to a true understanding of the charge distribution and also about magnetization of Mn atoms.

Figure 10 also shows a wide range of PDOS for all occupied *d*-orbitals, which could be a reason that why the onsite electron-electron repulsion parameter *U* is not very large in this system.

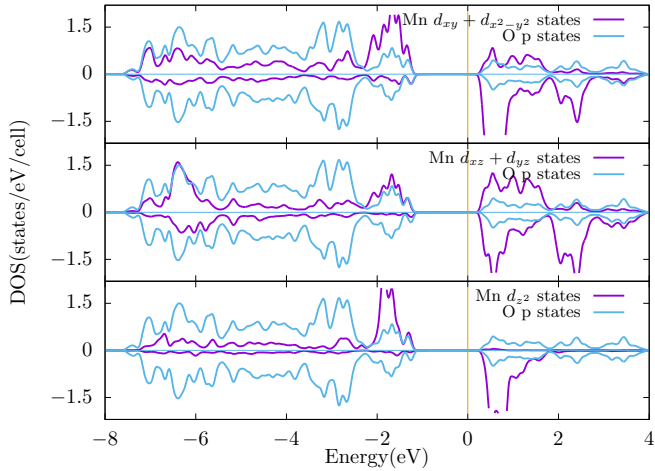


FIG. 10. Projected Density of States (PDOS) of Mn-*d* and O-*p* orbitals.

EXCHANGE CONSTANTS

In the experimental structure of Bi₃Mn₄O₁₂(NO₃) [1] (with *P*3 space group), within the experimental error, vertical positions of Mn atoms in the unit cell are almost equal (Table III). In the DFT calculations, we found that Mn₁ and Mn₂ as well as Mn₃ and Mn₄ do not have exactly the same vertical positions, even if exact site geometry optimization is performed. However, as Table III shows, in DFT, the vertical positions of Mn₁ and Mn₂ and also Mn₃ and Mn₄ are very close. The site geometry optimization has been done within 0.001 eV/Ång accuracy. The space group of geometry optimization structure and experimental structure is the same (P3, No 143). So the space group of Bi₃Mn₄O₁₄ doesn't change during geometry optimization.

Since Mn atoms are not completely identical, we have to use more Heisenberg constants. For example, instead of only one *J*₁ for first nearest neighbor interaction we need to consider two: one between Mn₁ and Mn₂ (*J*₁^{1,2}) and the other between Mn₃ and Mn₄ (*J*₁^{3,4}). For the second neighbor couplings *J*₂ we also have *J*₂^{1,1}, *J*₂^{2,2}, *J*₂^{3,3} and *J*₂^{4,4}. Similarly, there are variety of couplings for other inter and intra layer exchange interactions (see Table. IV).

To calculate the couplings of the Heisenberg Hamiltonian, we use 54 magnetic configurations listed in Table. VI. Employing the least square method by considering these 54 magnetic configurations, enables us to calculate the magnetic exchanges the within accuracy of 0.02 meV.

The ab initio results for the exchange couplings are given in Table. IV. These results are obtained after performing geometry optimization in a ferromagnetic configuration. The differences between the couplings of the same range are small (~ 0.1 meV), hence their arithmetic mean are reported in the main paper.

Using the experimental structure, the difference between the couplings of the same range are significant (see Table V). For example, $J_1^{1,2}=27.4$ meV $J_1^{3,4}=10.8$ meV within GGA/FPLO method. So assuming identical Mn atoms for experimental structure to derive J_{ij} are completely wrong.

In the main paper we assumed that the interaction between successive double layers could be ignored. To verify this assumption we calculate the energy difference of two magnetic configurations, a ferromagnetic configuration in which all the spins in all the bilayers are parallel and an anti-ferromagnetic configuration in which the spins in each bilayer are parallel, while they are antiparallel to the ones in neighboring bilayers. This energy difference gives an estimate of the strength of interaction between separated bilayers. Using FPLO method with *U* = 1.5 eV, we obtain an energy difference (per Mn atom) of ~ 0.3 meV for these two configurations. This value is an order

TABLE III. Experiment and DFT Wycoff position of Mn atoms. The DFT calculation is done with $U = 1.5\text{eV}$ by FPLO method.

| aotm | Experiment Wycoff position | | | DFT Wycoff position | | |
|-----------------|----------------------------|-----|----------|---------------------|-----|----------|
| | x | y | z | x | y | z |
| Mn ₁ | 2/3 | 1/3 | 0.855(5) | 2/3 | 1/3 | 0.855500 |
| Mn ₂ | 1/3 | 2/3 | 0.852(6) | 1/3 | 2/3 | 0.855979 |
| Mn ₃ | 2/3 | 1/3 | 0.218(5) | 2/3 | 1/3 | 0.233593 |
| Mn ₄ | 1/3 | 2/3 | 0.223(6) | 1/3 | 2/3 | 0.233109 |

of magnitude less than the minimum energy difference (per Mn atom) of 54 magnetic configurations inside each bilayer with respect to the ferromagnetic reference state, which is 6.6 meV (Fig. 3 of main paper). Therefore it would be safe to neglect the bilayer-bilayer interaction.

MAGNETIC CONFIGURATIONS

In this section, we show the 54 magnetic configurations used for the calculations of the Heisenberg coupling constants. To represent magnetic configurations, we assign a number on each Mn atoms in the $2 \times 2 \times 1$ supercell of $\text{Bi}_3\text{Mn}_4\text{O}_{12}(\text{NO}_3)$ (figure 11), and then we specify the direction of Mn magnetic moments (up or down) by arrows shown in Table. VI.

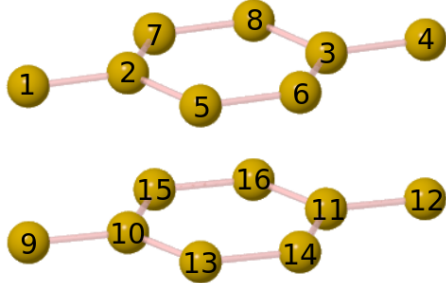


FIG. 11. Each Mn atoms are labeled by a number in $2 \times 2 \times 1$ supercell of $\text{Bi}_3\text{Mn}_4\text{O}_{12}(\text{NO}_3)$

DMRG RESULTS ANALYSIS

We use density matrix renormalization group (DMRG) techniques based on a matrix product state (MPS) representation to evaluate the spin correlation functions. MPS is an variational ansatz that the variational parameters can be controlled by the matrix size, M , called the bond dimension. The ground state converges after sweeping a few times through the system.

We carry out 10 sweeps to converge the ground state within an error less than 3 percent near the phase transition point. Moreover, we compare the correlation functions calculated using different bond dimension and find that the error of the results is less than 1.3 percent. Away from the phase transition point, the errors are less than these values and reach to 0.4 percent.

* shahbazi@cc.iut.ac.ir

- [1] O. Smirnova, M. Azuma, N. Kumada, Y. Kusano, M. Matsuda, Y. Shimakawa, T. Takei, Y. Yonesaki, and N. Kinomura, *Journal of the American Chemical Society* **131**, 8313 (2009).
- [2] N. Onishi, K. Oka, M. Azuma, Y. Shimakawa, Y. Motome, T. Taniguchi, M. Hiraishi, M. Miyazaki, T. Matsuda, A. Koda, *et al.*, *Physical Review B* **85**, 184412 (2012).
- [3] M. Matsuda, M. Azuma, M. Tokunaga, Y. Shimakawa, and N. Kumada, *Phys. Rev. Lett.* **105**, 187201 (2010).
- [4] S. Okubo, F. Elmasry, W. Zhang, M. Fujisawa, T. Sakurai, H. Ohta, M. Azuma, O. A. Smirnova, and N. Kumada, *Journal of Physics: Conference Series* **200**, 022042 (2010).
- [5] H. C. Kandpal and J. van den Brink, *Physical Review B* **83**, 140412 (2011).
- [6] R. Ganesh, D. Sheng, Y.-J. Kim, and A. Paramekanti, *Physical Review B* **83**, 144414 (2011).
- [7] R. Ganesh, S. V. Isakov, and A. Paramekanti, *Physical Review B* **84**, 214412 (2011).
- [8] J. Oitmaa and R. Singh, *Physical Review B* **85**, 014428 (2012).
- [9] S. Okubo, T. Ueda, H. Ohta, W. Zhang, T. Sakurai, N. Onishi, M. Azuma, Y. Shimakawa, H. Nakano, and T. Sakai, *Phys. Rev. B* **86**, 140401 (2012).
- [10] H. Zhang, M. Arlego, and C. Lamas, *Physical Review B* **89**, 024403 (2014).
- [11] F. G. Albaracín and H. Rosales, *Physical Review B* **93**, 144413 (2016).
- [12] R. Bishop and P. Li, arXiv preprint arXiv:1611.03287 (2016).
- [13] K. Koepernik and H. Eschrig, *Phys. Rev. B* **59**, 1743 (1999).
- [14] P. Giannozzi *et al.*, *Journal of Physics: Condensed Matter* **21**, 395502 (2009).
- [15] J. P. Perdew, K. Burke, and M. Ernzerhof, *Phys. Rev. Lett.* **77**, 3865 (1996).
- [16] V. I. Anisimov, J. Zaanen, and O. K. Andersen, *Phys. Rev. B* **44**, 943 (1991).
- [17] V. I. Anisimov, I. V. Solovyev, M. A. Korotin, M. T. Czyzyk, and G. A. Sawatzky, *Phys. Rev. B* **48**, 16929 (1993).
- [18] A. I. Liechtenstein, V. I. Anisimov, and J. Zaanen, *Phys. Rev. B* **52**, R5467 (1995).
- [19] H. Eschrig, K. Koepernik, and I. Chaplygin, *Journal of Solid State Chemistry* **176**, 482 (2003), special issue on The Impact of Theoretical Methods on Solid-State Chemistry.
- [20] See Supplementary Material at [URL].
- [21] A. O. de-la Roza, E. R. Johnson, and V. Luoa, *Computer Physics Communications* **185**, 1007 (2014).
- [22] A. O. de-la Roza, M. Blanco, A. M. Pends, and V. Luoa, *Computer Physics Communications* **180**, 157 (2009).
- [23] M. Dolfi, B. Bauer, S. Keller, A. Kosenkov, T. Ewart, A. Kantian, T. Giamarchi, and M. Troyer, *Computer Physics Communications* **185**, 3430 (2014).

TABLE IV. Heisenberg constants obtained by ab initio calculations (LDA+ U) using FPLO. The structure, which is used in these calculations, is derived from geometry optimization of $\text{Bi}_3\text{Mn}_4\text{O}_{12}(\text{NO}_3)$ in its ferromagnetic state.

| method | U | $J_1^{1,2}$ | $J_1^{3,4}$ | $J_2^{1,1}$ | $J_2^{2,2}$ | $J_2^{3,3}$ | $J_2^{4,4}$ | $J_3^{(1,2)}$ | $J_3^{3,4}$ | $J_{1c}^{1,3}$ | $J_{1c}^{2,4}$ | $J_{2c}^{1,3}$ | $J_{2c}^{2,4}$ | $J_{3c}^{1,3}$ | $J_{3c}^{2,4}$ | $J_{4c}^{1,3}$ | $J_{4c}^{2,4}$ |
|--------|-----|-------------|-------------|-------------|-------------|-------------|-------------|---------------|-------------|----------------|----------------|----------------|----------------|----------------|----------------|----------------|----------------|
| FPLO | 1.5 | 10.8 | 10.7 | 1.0 | 0.8 | 1.0 | 0.8 | 1.2 | 1.2 | 2.9 | 3.0 | 1.1 | 1.1 | 0.5 | 0.6 | 0.9 | 0.9 |
| | 2.0 | 9.0 | 9.0 | 0.9 | 0.7 | 0.9 | 0.7 | 1.0 | 1.0 | 2.6 | 2.6 | 1.0 | 0.9 | 0.4 | 0.5 | 0.8 | 0.8 |
| | 3.0 | 6.6 | 6.6 | 0.7 | 0.6 | 0.7 | 0.6 | 0.8 | 0.8 | 2.0 | 2.1 | 0.7 | 0.7 | 0.3 | 0.4 | 0.6 | 0.6 |
| | 4.0 | 5.1 | 5.1 | 0.5 | 0.4 | 0.5 | 0.5 | 0.6 | 0.7 | 1.6 | 1.7 | 0.6 | 0.6 | 0.3 | 0.3 | 0.5 | 0.5 |

TABLE V. Heisenberg constants obtained by ab initio calculations (LDA+ U) using different U and different methods. The experimental structure is used in these calculations.

| method | U | $J_1^{1,2}$ | $J_1^{3,4}$ | $J_2^{1,1}$ | $J_2^{2,2}$ | $J_2^{3,3}$ | $J_2^{4,4}$ | $J_3^{1,2}$ | $J_3^{3,4}$ | $J_{1c}^{1,3}$ | $J_{1c}^{2,4}$ | $J_{2c}^{1,3}$ | $J_{2c}^{2,4}$ | $J_{3c}^{1,3}$ | $J_{3c}^{2,4}$ | $J_{4c}^{1,3}$ | $J_{4c}^{2,4}$ |
|--------|-----|-------------|-------------|-------------|-------------|-------------|-------------|-------------|-------------|----------------|----------------|----------------|----------------|----------------|----------------|----------------|----------------|
| FPLO | 0.0 | 27.4 | 10.8 | 0.9 | 0.7 | 2.5 | 2.0 | 1.2 | 2.2 | 4.6 | 5.9 | 1.8 | 1.3 | 0.2 | 0.6 | 1.0 | 0.7 |
| | 2.0 | 18.4 | 6.5 | 0.6 | 0.5 | 1.6 | 1.4 | 0.8 | 1.3 | 2.7 | 3.6 | 1.2 | 1.0 | 0.3 | 0.6 | 0.9 | 0.7 |
| | 3.0 | 14.1 | 4.3 | 0.5 | 0.4 | 1.2 | 1.1 | 0.6 | 1.0 | 2.2 | 2.8 | 0.9 | 0.8 | 0.3 | 0.4 | 0.7 | 0.5 |
| | 4.0 | 11.1 | 2.8 | 0.3 | 0.3 | 1.0 | 0.8 | 0.5 | 0.8 | 1.7 | 2.3 | 0.7 | 0.6 | 0.2 | 0.3 | 0.5 | 0.4 |

TABLE VI. 54 magnetic configurations which are used to derive J_{ij} .

| Magnetic configuration | Mn ₁ | Mn ₂ | Mn ₃ | Mn ₄ | Mn ₅ | Mn ₆ | Mn ₇ | Mn ₈ | Mn ₉ | Mn ₁₀ | Mn ₁₁ | Mn ₁₂ | Mn ₁₃ | Mn ₁₄ | Mn ₁₅ | Mn ₁₆ |
|------------------------|-----------------|-----------------|-----------------|-----------------|-----------------|-----------------|-----------------|-----------------|-----------------|------------------|------------------|------------------|------------------|------------------|------------------|------------------|
| 1 | ↑ | ↑ | ↑ | ↑ | ↑ | ↑ | ↑ | ↑ | ↑ | ↑ | ↑ | ↑ | ↑ | ↑ | ↑ | ↑ |
| 2 | ↑ | ↑ | ↓ | ↓ | ↑ | ↑ | ↓ | ↑ | ↑ | ↑ | ↓ | ↑ | ↑ | ↓ | ↑ | ↓ |
| 3 | ↑ | ↓ | ↓ | ↑ | ↑ | ↑ | ↑ | ↑ | ↑ | ↓ | ↑ | ↑ | ↑ | ↑ | ↑ | ↑ |
| 4 | ↑ | ↓ | ↑ | ↑ | ↑ | ↑ | ↑ | ↑ | ↑ | ↑ | ↑ | ↑ | ↑ | ↑ | ↑ | ↑ |
| 5 | ↓ | ↓ | ↑ | ↑ | ↑ | ↑ | ↑ | ↑ | ↑ | ↓ | ↑ | ↑ | ↑ | ↑ | ↑ | ↑ |
| 6 | ↑ | ↑ | ↑ | ↓ | ↓ | ↑ | ↑ | ↓ | ↑ | ↑ | ↑ | ↑ | ↑ | ↑ | ↑ | ↑ |
| 7 | ↑ | ↑ | ↑ | ↓ | ↓ | ↓ | ↓ | ↓ | ↑ | ↑ | ↑ | ↑ | ↑ | ↑ | ↑ | ↑ |
| 8 | ↑ | ↓ | ↑ | ↑ | ↑ | ↓ | ↓ | ↑ | ↑ | ↑ | ↑ | ↑ | ↑ | ↑ | ↑ | ↑ |
| 9 | ↑ | ↑ | ↑ | ↑ | ↑ | ↑ | ↑ | ↓ | ↑ | ↑ | ↑ | ↑ | ↑ | ↑ | ↑ | ↑ |
| 10(N ₁) | ↑ | ↓ | ↑ | ↑ | ↓ | ↑ | ↓ | ↑ | ↓ | ↑ | ↓ | ↑ | ↓ | ↑ | ↓ | ↑ |
| 11 | ↓ | ↓ | ↓ | ↑ | ↑ | ↓ | ↓ | ↑ | ↑ | ↓ | ↑ | ↑ | ↑ | ↑ | ↑ | ↑ |
| 12 | ↓ | ↓ | ↓ | ↓ | ↓ | ↑ | ↑ | ↑ | ↑ | ↑ | ↓ | ↑ | ↑ | ↑ | ↑ | ↑ |
| 13 | ↓ | ↓ | ↓ | ↓ | ↓ | ↓ | ↑ | ↑ | ↑ | ↑ | ↓ | ↑ | ↑ | ↑ | ↑ | ↑ |
| 14 | ↓ | ↓ | ↓ | ↓ | ↓ | ↓ | ↓ | ↑ | ↑ | ↑ | ↑ | ↑ | ↑ | ↑ | ↑ | ↑ |
| 15 | ↑ | ↑ | ↑ | ↑ | ↑ | ↑ | ↑ | ↑ | ↑ | ↑ | ↑ | ↑ | ↑ | ↑ | ↑ | ↑ |
| 16 | ↑ | ↑ | ↑ | ↓ | ↓ | ↑ | ↓ | ↑ | ↓ | ↑ | ↑ | ↑ | ↑ | ↑ | ↑ | ↑ |
| 17 | ↓ | ↓ | ↓ | ↓ | ↓ | ↓ | ↑ | ↑ | ↑ | ↑ | ↓ | ↑ | ↑ | ↑ | ↑ | ↑ |
| 18 | ↓ | ↓ | ↓ | ↓ | ↓ | ↓ | ↓ | ↑ | ↑ | ↑ | ↓ | ↑ | ↑ | ↑ | ↑ | ↑ |
| 19 | ↑ | ↑ | ↑ | ↑ | ↑ | ↑ | ↑ | ↑ | ↑ | ↑ | ↑ | ↑ | ↑ | ↑ | ↑ | ↑ |
| 20 | ↑ | ↑ | ↓ | ↓ | ↑ | ↓ | ↓ | ↑ | ↓ | ↑ | ↓ | ↓ | ↑ | ↑ | ↑ | ↑ |
| 21 | ↑ | ↑ | ↓ | ↑ | ↑ | ↑ | ↓ | ↑ | ↓ | ↑ | ↓ | ↑ | ↓ | ↑ | ↑ | ↑ |
| 22 | ↓ | ↓ | ↓ | ↓ | ↓ | ↓ | ↓ | ↑ | ↑ | ↑ | ↑ | ↑ | ↑ | ↑ | ↑ | ↑ |
| 23 | ↑ | ↑ | ↑ | ↓ | ↓ | ↓ | ↓ | ↑ | ↑ | ↑ | ↓ | ↑ | ↑ | ↑ | ↑ | ↑ |
| 24 | ↑ | ↑ | ↑ | ↓ | ↓ | ↑ | ↑ | ↑ | ↑ | ↑ | ↓ | ↑ | ↑ | ↑ | ↑ | ↑ |
| 25 | ↓ | ↑ | ↑ | ↓ | ↓ | ↑ | ↓ | ↓ | ↓ | ↑ | ↓ | ↑ | ↑ | ↑ | ↑ | ↑ |
| 26 | ↑ | ↑ | ↑ | ↑ | ↓ | ↓ | ↓ | ↑ | ↑ | ↑ | ↑ | ↑ | ↑ | ↑ | ↑ | ↑ |
| 27 | ↑ | ↑ | ↑ | ↑ | ↓ | ↓ | ↓ | ↑ | ↓ | ↑ | ↓ | ↑ | ↑ | ↑ | ↑ | ↑ |
| 28(N ₂) | ↑ | ↓ | ↑ | ↑ | ↓ | ↓ | ↑ | ↓ | ↑ | ↓ | ↑ | ↓ | ↑ | ↓ | ↑ | ↑ |
| 29 | ↓ | ↓ | ↓ | ↓ | ↓ | ↓ | ↑ | ↓ | ↑ | ↓ | ↑ | ↓ | ↑ | ↓ | ↑ | ↑ |
| 30 | ↓ | ↓ | ↓ | ↓ | ↓ | ↓ | ↓ | ↑ | ↑ | ↓ | ↑ | ↓ | ↑ | ↓ | ↑ | ↑ |
| 31 | ↓ | ↓ | ↑ | ↓ | ↓ | ↓ | ↓ | ↑ | ↑ | ↑ | ↓ | ↑ | ↓ | ↑ | ↓ | ↑ |
| 32 | ↑ | ↑ | ↑ | ↑ | ↑ | ↑ | ↑ | ↓ | ↓ | ↑ | ↑ | ↑ | ↑ | ↑ | ↑ | ↑ |
| 33 | ↑ | ↑ | ↑ | ↑ | ↑ | ↑ | ↓ | ↑ | ↓ | ↑ | ↓ | ↑ | ↓ | ↑ | ↓ | ↑ |
| 34 | ↓ | ↓ | ↓ | ↑ | ↑ | ↑ | ↓ | ↑ | ↓ | ↑ | ↓ | ↑ | ↓ | ↑ | ↓ | ↑ |
| 35 | ↓ | ↓ | ↑ | ↑ | ↑ | ↓ | ↓ | ↑ | ↓ | ↑ | ↓ | ↑ | ↓ | ↑ | ↓ | ↑ |
| 36 | ↓ | ↓ | ↑ | ↑ | ↓ | ↓ | ↓ | ↑ | ↓ | ↑ | ↑ | ↑ | ↑ | ↑ | ↑ | ↑ |
| 37 | ↓ | ↓ | ↓ | ↑ | ↑ | ↑ | ↑ | ↓ | ↑ | ↑ | ↓ | ↑ | ↑ | ↑ | ↑ | ↑ |
| 38 | ↑ | ↑ | ↑ | ↑ | ↑ | ↑ | ↑ | ↓ | ↑ | ↑ | ↓ | ↑ | ↑ | ↑ | ↑ | ↑ |
| 39 | ↑ | ↑ | ↓ | ↓ | ↑ | ↓ | ↓ | ↑ | ↓ | ↑ | ↓ | ↑ | ↓ | ↑ | ↓ | ↑ |
| 40 | ↑ | ↑ | ↓ | ↓ | ↑ | ↑ | ↑ | ↑ | ↑ | ↑ | ↓ | ↑ | ↓ | ↑ | ↓ | ↑ |
| 41 | ↓ | ↑ | ↑ | ↑ | ↑ | ↑ | ↓ | ↑ | ↓ | ↑ | ↓ | ↑ | ↓ | ↑ | ↓ | ↑ |
| 42 | ↑ | ↑ | ↑ | ↑ | ↑ | ↓ | ↓ | ↓ | ↑ | ↓ | ↑ | ↓ | ↑ | ↓ | ↑ | ↓ |
| 43 | ↑ | ↑ | ↑ | ↑ | ↓ | ↓ | ↓ | ↑ | ↑ | ↓ | ↑ | ↓ | ↑ | ↓ | ↑ | ↓ |
| 44 | ↓ | ↑ | ↑ | ↑ | ↑ | ↓ | ↓ | ↑ | ↑ | ↓ | ↑ | ↓ | ↑ | ↓ | ↑ | ↓ |
| 45 | ↓ | ↑ | ↑ | ↑ | ↑ | ↓ | ↓ | ↑ | ↑ | ↓ | ↑ | ↓ | ↑ | ↓ | ↑ | ↓ |
| 46 | ↑ | ↑ | ↑ | ↑ | ↓ | ↓ | ↓ | ↑ | ↑ | ↓ | ↑ | ↓ | ↑ | ↓ | ↑ | ↓ |
| 47(N ₃) | ↑ | ↑ | ↑ | ↑ | ↑ | ↑ | ↑ | ↑ | ↑ | ↑ | ↑ | ↑ | ↑ | ↑ | ↑ | ↑ |
| 48 | ↓ | ↓ | ↓ | ↓ | ↓ | ↓ | ↓ | ↑ | ↓ | ↑ | ↓ | ↑ | ↓ | ↓ | ↑ | ↑ |
| 49 | ↑ | ↓ | ↓ | ↓ | ↑ | ↓ | ↓ | ↑ | ↓ | ↑ | ↓ | ↑ | ↓ | ↓ | ↑ | ↓ |
| 50 | ↓ | ↓ | ↑ | ↑ | ↓ | ↓ | ↑ | ↑ | ↓ | ↑ | ↓ | ↑ | ↓ | ↑ | ↓ | ↑ |
| 51 | ↑ | ↑ | ↑ | ↓ | ↓ | ↑ | ↑ | ↓ | ↑ | ↓ | ↑ | ↓ | ↑ | ↓ | ↑ | ↓ |
| 52 | ↓ | ↑ | ↑ | ↓ | ↓ | ↑ | ↑ | ↓ | ↑ | ↓ | ↑ | ↓ | ↑ | ↓ | ↑ | ↓ |
| 53 | ↑ | ↑ | ↑ | ↓ | ↑ | ↑ | ↑ | ↓ | ↑ | ↑ | ↓ | ↑ | ↑ | ↓ | ↑ | ↓ |
| 54 | ↓ | ↑ | ↑ | ↓ | ↑ | ↑ | ↑ | ↓ | ↑ | ↑ | ↓ | ↑ | ↑ | ↑ | ↑ | ↑ |